Experimental and theoretical study of the photodissociation reaction of thiophenol at 243 nm: Intramolecular orbital alignment of the phenylthiyl radical

Ivan S. Lim, Jeong Sik Lim, Yoon Sup Lee, and Sang Kyu Kim[a)]
Department of Chemistry and School of Molecular Science (BK21), Korea Advanced Institute of Science and Technology (KAIST), Daejeon 305-701, Republic of Korea

(Received 4 October 2006; accepted 29 November 2006; published online 17 January 2007)

The photoinduced hydrogen (or deuterium) detachment reaction of thiophenol (C_6H_5SH) or thiophenol-d_1 (C_6H_5SD) pumped at 243 nm has been investigated using the H (D) ion velocity map imaging technique. Photodissociation products, corresponding to the two distinct and anisotropic rings observed in the H (or D) ion images, are identified as the two lowest electronic states of phenylthiyl radical ($C_6H_5S\cdot$). *Ab initio* calculations show that the singly occupied molecular orbital of the phenylthiyl radical is localized on the sulfur atom and it is oriented either perpendicular or parallel to the molecular plane for the ground (B_1) and the first excited state (B_2) species, respectively. The experimental energy separation between these two states is 2600 ± 200 cm^{-1} in excellent agreement with the authors' theoretical prediction of 2674 cm^{-1} at the CASPT2 level. The experimental anisotropy parameter (β) of -1.0 ± 0.05 at the large translational energy of D from the C_6H_5SD dissociation indicates that the transition dipole moment associated with this optical transition at 243 nm is perpendicular to the dissociating S–D bond, which in turn suggests an ultrafast $D+C_6H_5S\cdot(B_1)$ dissociation channel on a repulsive potential energy surface. The reduced anisotropy parameter of -0.76 ± 0.04 observed at the smaller translational energy of D suggests that the $D+C_6H_5S\cdot(B_2)$ channel may proceed on adiabatic reaction paths resulting from the coupling of the initially excited state to other low-lying electronic states encountered along the reaction coordinate. Detailed high level *ab initio* calculations adopting multireference wave functions reveal that the $C_6H_5S\cdot(B_1)$ channel may be directly accessed via a $^1(n_\pi,\sigma^*)$ photoexcitation at 243 nm while the key feature of the photodissociation dynamics of the $C_6H_5S\cdot(B_2)$ channel is the involvement of the $^3(n_\pi,\pi^*)\rightarrow{}^3(n_\sigma,\sigma^*)$ profile as well as the spin-orbit induced avoided crossing between the ground and the $^3(n_\pi,\sigma^*)$ state. The S–D bond dissociation energy of thiophenol-d_1 is accurately estimated to be $D_0=79.6\pm0.3$ kcal/mol. The S–H bond dissociation energy is also estimated to give $D_0=76.8\pm0.3$ kcal/mol, which is smaller than previously reported ones by at least 2 kcal/mol. The C–H bond of the benzene moiety is found to give rise to the H fragment. Ring opening reactions induced by the π-π^*/n_π-π^* transitions followed by internal conversion may be responsible for the isotropic broad translational energy distribution of fragments. © *2007 American Institute of Physics*. [DOI: 10.1063/1.2424939]

I. INTRODUCTION

Stereodynamics has been one of the most fascinating aspects in chemical dynamics. The steric factor has long been employed as an essential parameter in the formulation of theoretical rate constants based on the simple collision theory.[1,2] In order to investigate steric effects in chemical reactions, a number of brilliant experiments for the alignment and/or orientation of reactant molecules have been intensively carried out in recent decades.[3–32] Many successful examples have been reported for typical systems such as the bimolecular reaction between a metal atom with an oriented methyl iodide.[3–8,33] Accordingly, there exist may excellent review articles on this subject,[33–41] and the concept of such alignment will be briefly described here. As the so-called "cone of acceptance" is easily visualized for reactive collision experiments in which two reactants are relatively well oriented with respect to each other, the molecular alignment in the laboratory frame has been the subject most intensively investigated.[3–20] In many cases, the alignment of molecules has been achieved by using the interaction of the molecular permanent or transition dipole moments with a strong external electric field, often generated by the optical pumping,[8–15] which then manipulates the nuclear framework in the laboratory-fixed axes. This "laboratory-frame" alignment of the molecule, therefore, enables one to explore stereoselective chemistry in terms of a chemical shape along the direction of approach in bimolecular reactions.

A conceptually different kind of alignment is known for open-shell reactants where the relative orientation of the electronic orbital with respect to the direction of bimolecular collision plays a critical role in stereoselective chemical reactivity. Such an electronic orbital alignment can be achieved

[a)]Author to whom correspondence should be addressed. Electronic mail: sangkyukim@kaist.ac.kr

in three different processes:[35] (a) precollision alignment, (b) in-collision alignment, and (c) postcollision alignment. In the precollision alignment, for example, atomic orbital angular momentum is aligned in the laboratory frame by the polarized laser pulse.[16–20] For in-collision alignment, electronic states of the collision pair prepared in the form of the van der Waals complex is specifically selected.[21,22] In the postcollision alignment, the electronic orbital is aligned either in the laboratory or recoil frame subsequent to the reactive (or inelastic) collision, photodissociation, or gas-surface collision.[23–31] Typically, atoms and diatomic molecules have been subjected to such experiments. For instance, the relative population in Λ-doublet states of diatomic fragments such as $OH(\cdots\sigma^2\pi^3;X\,^2\Pi)$, $NO(\cdots\sigma^2\pi^1;X\,^2\Pi)$, and $NH^*(\cdots\sigma^1\pi^3;c\,^1\Pi)$ has long been utilized as a clue for determining the planarity of the photodissociation process.[28–31] This is aided by the fact that the singly occupied electronic orbital, in the classical limit, is either parallel or perpendicular to the rotating plane. The orbital angular momentum may be relatively well defined along the molecular axis for linear polyatomic molecules. However, for other polyatomics containing conjugated molecular fragments such as a benzene ring, there usually occurs a strong conjugation between the molecular frame (i.e., benzene ring) and the substituents, which results in the ill-defined orbital angular momentum with respect to the symmetry species. For example, it is well known that the oxygen lone pair in phenol exhibits a considerable amount of π interaction with the adjacent benzene ring.[42,43]

One may consider yet another kind of orbital alignment which may be classified as a "postcollision" alignment process. Here, an intramolecular orbital alignment is achieved in the molecular frame defined by symmetry rather than in the laboratory or recoil frame such as a rotating plane. For example, the π and σ structures of hydrogen-abstracted planar aromatic radicals give rise to molecular orbitals aligned with respect to a molecular frame defined by the benzene moiety. The energetic ordering of such radical species enforced by the symmetry-allowed crossing of A'' and A' states of the parent neutral molecule (i.e., the respective π and σ structures of the radical) has, in fact, been predicted almost three decades ago.[44] In particular, phenol and related compounds have received a considerable amount of interest as a prototype of aromatic biomolecules. It is now well accepted that in the photochemistry of phenol and other planar aromatic systems, the ground $^1A'$ state correlates asymptotically to the electronically excited $^2\sigma$ state of the phenoxyl radical and the excited $^1A''$ of the parent molecule to the ground $^2\pi$ state of the radical species.[45–48] Theoretical investigations of the photoinduced hydrogen detachment, which has only become available recently, provide an intuitive account of the photodissociation dynamics of phenol.[45–47]

As for thiol compounds, there is a fruitful amount of studies available such as for those of H_2S (Refs. 49–56) and CH_3SH.[57–60] To the best of our knowledge, however, aromatic thiophenol has rarely been studied and as a result no detailed information on the photodissociation process of the hydrogen detachment reaction is available. We note a photodissociation study of $C_6H_5SH \rightarrow C_6H_5+SH$ channel at 193 nm by Nourbakhsh *et al.*[61] An interesting feature of the hydrogen-detached phenylthiyl radical is that both the excited triplet states as well as the singlet state could easily generate the radical species. In light of this, we investigated the photodissociation of jet-cooled C_6H_5SH (C_6H_5SD) at 243 nm and presented the first experimental evidence for the photoinduced products of phenylthiyl radical species characterized by specifically chosen molecular orbital alignment with respect to the benzene moiety. In this paper we intend to give a full experimental account of our previous Communication.[62] Furthermore, we elaborate on the previous theoretical investigation and provide some clues as to the minimum energy pathways for the hydrogen detachment reaction of thiophenol. Novel aspects of the thiophenol photodissociation process, which are crucial for the interpretation of the observed experimental data, are revealed through detailed multireference *ab initio* calculations.

II. EXPERIMENT

Only a brief description of the experimental setup for the velocity map ion imaging is given below as a more extensive detail has been described elsewhere.[63] A differentially pumped vacuum chamber equipped with two turbomolecular pumps (Varian 550) was used for the preparation of the supersonic jet and molecular ionization/detection. An ~5% mixture of thiophenol (Aldrich) in He was expanded through a nozzle orifice (General Valve 9 series, 0.3 mm diameter) into vacuum with a backing pressure of approximately 3 atm. The nozzle was heated to 65 °C and was operated at a 10 Hz repetition. The resultant supersonic jet was skimmed through a 1 mm diameter skimmer before being overlapped with the laser pulse. The third harmonic output of a neodymium doped yttrium aluminum garnet laser (Spectra-Physics, GR150) was used to pump a dye laser (Lambda Physik, Scanmate2) to generate the laser pulse at 242–244 nm after frequency doubling through a beta barium borate crystal placed on a homemade autotracker. Deuterium-substituted thiophenol (C_6H_5SD) was prepared by mixing D_2O with thiophenol dissolved in ether, which was stirred vigorously for the H/D substitution. This process was repeated several times before the C_6H_5SD enriched thiophenol compound was extracted from the ether solvent. But, because of the incomplete H/D substitution, the mixture with ~80% of thiophenol-d_1 was used. The hydrogen (or deuterium) generated by the photodissociation of thiophenol at 243 nm was ionized by (2+1) resonance-enhanced ionization by the same laser pulse used for excitation. These ions were repelled, accelerated on the ion optics carefully aligned for the velocity mapping condition, and detected on a position sensitive detector equipped with dual microchannel plates with a P20 phosphor screen (Burle, 3040 FM CT, 40 mm diameter). The polarization of the laser pulse was perpendicular to the time-of-flight axis, while it was parallel to the position sensitive detector plane. The wavelength of the laser pulse was continuously scanned over the entire Doppler width of the H/D ionization transition while the image was being taken and averaged over 36 000 laser shots. Images were recorded by a charge-coupled device camera

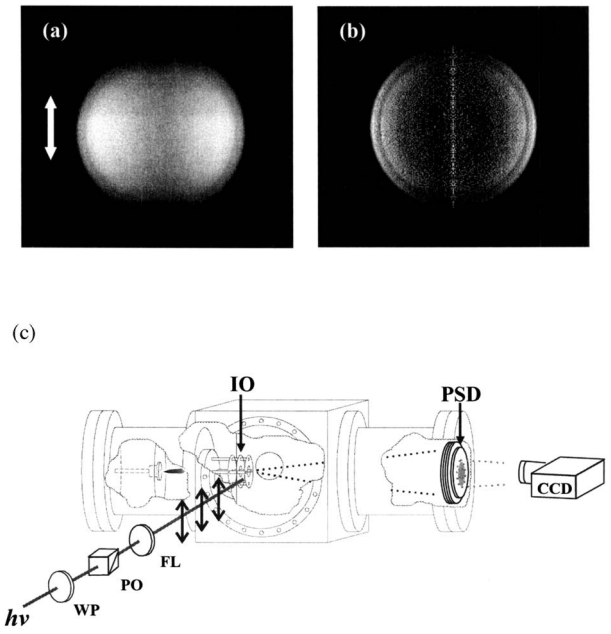

FIG. 1. (a) 2D projection of the 3D spatial distribution of D ion, (b) the center slice of the reconstructed 3D distribution, and (c) experimental setup used. The vertical arrow in (a) and (c) indicates the polarization of the pump laser. M: mirror, FL: focusing lens, PO: polarizing optics, IO: ion optics, and PSD: position sensitive detector.

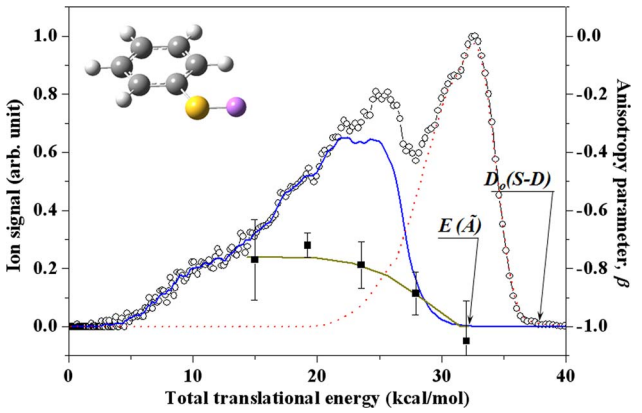

FIG. 2. (Color online) The total translational energy distribution and associated anisotropy parameter. Open circles are showing the total translation energy distribution, while the (red) dotted and (blue) solid lines represent the translational energy distribution for the $D+C_6H_5S\cdot(B_1)$ and $D+C_6H_5S\cdot(B_2)$ channels, respectively. The averaged anisotropy parameter as a function of the total translation energy is shown as the filled rectangle and used for the deconvolution of the translational energy distribution (see the text).

(Hammamatsu) using a gravity event counting method. Three-dimensional images were constructed from two-dimensional raw images using the basis-set expansion (BASEX) algorithm.[64] Speed and angular distributions of the fragments extracted from the images were calibrated based on a controlled experiment on the O_2 photodissociation for which the energetics have been well documented.[65]

III. COMPUTATIONAL DETAILS

Molecular geometry optimization for the construction of potential energy curves as a function of S–H coordinate was performed at the CASSCF level with respect to the ground state gradients. The active space in CASSCF are six electrons in six orbitals composed of the highest occupied and lowest unoccupied σ orbitals between S and H and two pairs of π bonding and antiorbitals on benzene. All degrees of freedom were relaxed during optimization except for a few cases where oscillatory behavior was observed near the intersection of electronic states under consideration. This presented no further difficulty in the construction of potential energy curves as the rather uncharacteristic geometric parameters (i.e., those for the benzene ring) do not alter significantly to cause a quantitative problem in the final results. Dynamic correlation effects were accounted for at the multireference configuration interaction (MRCI) level for the potential energy profile. Where spin-orbit effects were considered, a state averaged MRCI procedure was adopted. Vertical excitation energies at the ground state equilibrium geometry for selected states were obtained at the complete active space second order perturbation theory (CASPT2) level. Density functional theory (DFT) calculations were also carried out for comparison of vertical excitation energies. The basis set used in all calculations was 6-31G**. All calculations were performed with GAUSSIAN03 (Ref. 66) and MOLPRO (Ref. 67) program packages.

Before leaving this section we briefly mention that the planar structure of thiophenol with S–H fragment oriented parallel to the benzene plane is found to lie lower in energy by 0.75 kcal/mol than the one with S–H perpendicular to benzene at the DFT level (B3LYP/6-31G**). The ground state geometry therefore adopts a planar geometry in a C_s symmetry where the plane containing the benzene ring is defined as the xy plane and the C–S bond is along the x axis. For the radical, we used a C_{2v} point group where the main two-fold z axis is placed along the C–S bond and the molecule lies in the yz plane. We do not give in this report detailed geometry parameters, which will be made available upon request.

IV. RESULTS AND DISCUSSION

A. Translational energy distribution and anisotropy parameters of the D fragment in the photodissociation of C_6H_5SD at 243 nm

Raw and reconstructed images of the D ion from the photodissociation of C_6H_5SD at 243 nm are shown in Figs. 1(a) and 1(b), respectively. The two-dimensional (2D) projection of the raw three-dimensional (3D) distribution in Fig. 1(a) has been reconstructed by the BASEX algorithm[64] to give the center slice of the 3D distribution of the D fragment in Fig. 1(b). Clearly, both images consist of two distinct anisotropic rings corresponding to the two different translational energies. From the reconstructed image, the total translational energy distribution is extracted using the following relation:

$$E_T^{\text{tot}} = \frac{m_{C_6H_5S} + m_D}{m_{C_6H_5S}} E_T^D, \quad (1)$$

where E_T^{tot} is the total transitional energy, E_T^D the kinetic energy of the D fragment, and $m_D/m_{C_6H_5S}$ the masses of the respective deuterium/phenylthiyl fragments. An appropriate Jacobian ($dv/dE \propto 1/v$) was applied to convert the velocity distribution to the translational energy distribution, $P(E_T)$. Figure 2 depicts the resulting total translational energy distribution. Also plotted in the figure is the angular distribution of the D fragment represented by the anisotropy parameter (β) which is extracted from the D atom images analyzed by the BASEX algorithm[64] using the relation below,

$$I(\theta) \propto [1 + \beta P_2(\cos\theta)]. \quad (2)$$

Here, θ is the angle between the pump laser polarization and the recoil velocity vector of the fragment, $P_2(x)$ the second order Legendre polynomial, and $I(\theta)$ is the signal intensity of the fragment ion as a function of θ.

Quite obviously, the total translational energy distribution undergoes little change from the D atom translational energy distribution as most of the translational energy goes to the D fragment due to the much smaller mass of D atom compared with that of $C_6H_5S\cdot$. A more interesting feature of photodissociation is revealed by the presence of a bimodal distribution with two distinct peaks located at 24.7 and 32.4 kcal/mol, corresponding to the inner and the outer rings of the velocity map image, respectively. Since there is no intrinsic internal energy for the D fragment, it is only natural to infer that the observed peaks arise from two different quantum states of phenylthiyl radical produced by photoinduced hydrogen detachment in thiophenol. Furthermore, the two distinctive anisotropy values obtained for $\beta=-1$ and $\beta=-0.76$ relating to the respective larger and the smaller translational energies indicate that there are at least two distinct dissociation pathways responsible for the two anisotropies at the observed peaks. This is also supported by the sharp transition around these two values. One may, therefore, safely exclude the possibility that the origin of the observed peaks is related to vibrational excitation of the radical as such a distinct bimodal distribution is not expected for the vibrational energy disposal of the polyatomic fragment with many vibrational degrees of freedom.[68,69] The sharp variation of β as a function of the translation energy in the middle part of the bimodal distribution also provides an excellent clue for the deconvolution of the measured translational energy distribution into two components with different anisotropies. The deconvolution is carried out based on the following relation:

$$\beta(E) = (-1.00)P_1(E) + (-0.76)P_2(E), \quad (3)$$

where $\beta(E)$ is the anisotropy parameter as a function of the translational energy E. $P_1(E)$ and $P_2(E)$ represent the respective population of the D fragment belonging to $\beta=-1.00$ and $\beta=-0.76$ channels with $P_1(E)+P_2(E)=1$. The deconvoluted distributions of each channel show the similar shape to each other though the distribution at the smaller energy is wider than that at the large translational energy (Fig. 2).

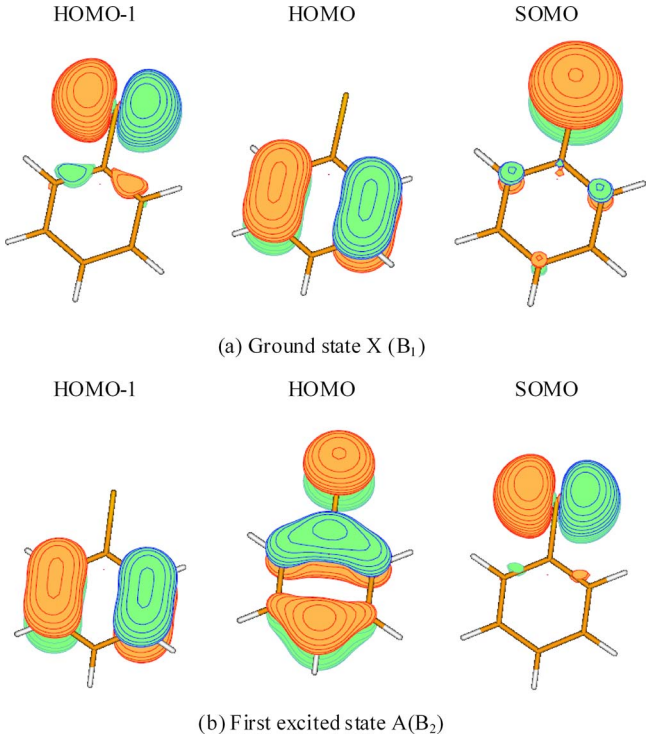

FIG. 3. (Color online) Natural orbitals for the singly occupied (SO) molecular orbital (MO), highest doubly occupied MO (HOMO), and second HOMO (HOMO-1) of the (a) ground state and the (b) first electronically excited state of thiophenol radical.

B. Molecule-frame orbital alignment of the phenylthiyl radical ($C_6H_5S\cdot$)

The experimental findings in the previous section strongly suggest that there exist at least two distinctive pathways leading to the formation of phenylthiyl radical species in two different electronic states. In fact, an early theoretical study at the single excitation configuration interaction level predicted two close-lying lowest electronic states $\tilde{X}$ and $\tilde{A}$ of the $C_6H_5S\cdot$ radical separated by $\sim$3200 cm^{-1}.[68] To the best of our knowledge, there is no experimentally determined energy separation for these states.[68–72] This is not surprising as the transition between the $\tilde{X}(B_1)$ and $\tilde{A}(B_2)$ states is optically forbidden. Nonetheless, one may still estimate such a quantity from the location of the observed peaks in the total translational energy distribution by taking the energy difference between the maximum translational energy of each states in the bimodal distribution as the energy difference between the two lowest electronic states of $C_6H_5S\cdot$ radical. This is based on the assumption that there are non-negligible products formed in the zero-point vibrational level of each state. The resulting $\tilde{A}\leftarrow\tilde{X}$ excitation energy of 2600 ± 200 cm^{-1} (*vide supra*) is in line with the earlier mentioned theoretical value. In strong support for the present experimental $\tilde{A}\leftarrow\tilde{X}$ excitation energy is our *ab initio* result obtained at the CASPT2 level, giving 2674 cm^{-1}. Spin-orbit effects are found to be rather small, which increases the excitation energy by about 25 cm^{-1}.

It has been argued before that the sulfur lone pair in thiophenol exhibits a considerable amount of π interaction with the benzene ring.[73] This was based on the relative mag-

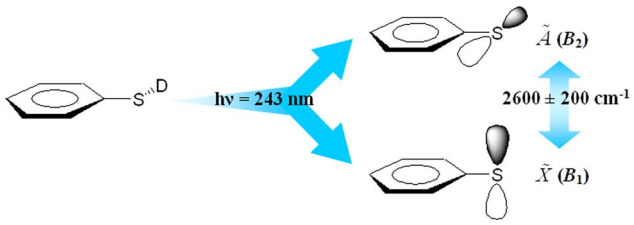

FIG. 4. (Color online) Schematic diagram showing that the photodissociation of C_6H_5SD gives rise to intermolecular orbital alignment.

nitude of the ionization potentials. Our *ab initio* calculation reveals that the both singly occupied molecular orbitals (SOMOs) for the $\tilde{X}$ and $\tilde{A}$ states of phenylthiyl are largely localized on the sulfur atom with little interaction with the adjacent benzene π orbitals, as shown in Fig. 3. In other words, the SOMOs are nonbonding characterized by the singly occupied $3p$ orbital on sulfur. This is also the case for the highest occupied molecular orbital (HOMO) of neutral thiophenol. The difference between the $\tilde{X}$ and $\tilde{A}$ states of phenylthiyl radical then results from the relative orientation of the singly occupied nonbonding orbital aligned with respect to the benzene plane. That is, the ground state $(\tilde{X})$ of the radical exhibits the out-of-plane SOMO, belonging to a B_1 representation and the excited state $(\tilde{A})$ the in-plane SOMO of a B_2 representation. Derived from this is a simplistic scheme for the generation of intramolecularly aligned orbital species or simply a "molecular frame orbital alignment" via the photodissociation of thiophenol at 243 nm, as depicted in Fig. 4.

It is worthwhile to investigate the branching ratio of two dissociation channels and energy partitioning in each channel as these can provide insights on the potential energy surfaces along the dissociation coordinate. From the deconvoluted translational energy distributions in Fig. 2, the branching ratio at 243 nm is estimated to be 1.00:1.31 for the $D+C_6H_5S\cdot(B_1)$ and $D+C_6H_5S\cdot(B_2)$ channels. The average of the translational energy is calculated to be 30.82 kcal/mol for the former and 18.58 kcal/mol for the latter. For the $D+C_6H_5S\cdot(B_1)$ channel, the available energy (E_{avl}) at 243 nm is 38.11±0.30 kcal/mol, which is obtained from the equation $E_{avl}=E_{h\nu}-D_0$. Here, $E_{h\nu}$ denotes the photon energy and D_0 does the S–D bond dissociation energy, estimated from the maximum value of the D translational energy distribution to be 79.6±0.3 kcal/mol, considering the initial internal energy of thiophenol in the supersonic jet which should be much smaller than 0.05 kcal/mol. The available energy for the $D+C_6H_5S\cdot(B_2)$ channel, on the other hand, is estimated from the relation $E_{avl}=E_{h\nu}-D_0-E_e$, where the energy difference (E_e) between $C_6H_5S\cdot(B_2)$ and $C_6H_5S\cdot(B_1)$ is

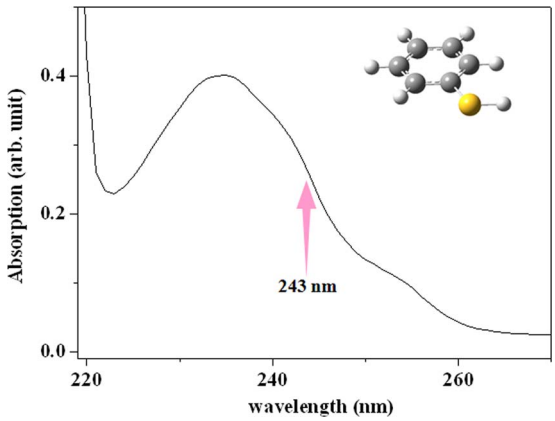

FIG. 5. (Color online) Absorption spectrum of thiophenol taken in *n*-hexanes. The pump energy of 243 nm used in this work is indicated as an arrow.

taken to be 2600±200 cm^{-1}. Therefore, the portionings of the available energy into the translational degree of freedom are estimated to be 80.9% and 60.6% for the $C_6H_5S\cdot(B_1)$ and $C_6H_5S\cdot(B_2)$ channels, respectively (see Table I). Different energy partitionings suggest that the potential energy curves for the two S–D dissociation channels along the S–D dissociation coordinate should be quite different from each other. The larger anisotropy parameter ($\beta=-1.00$) for the $D+C_6H_5S\cdot(B_1)$ channel indicates that the S–D bond rupture is prompt, which is consistent with the larger translational energy release. On the other hand, the reduced anisotropy parameter ($\beta=-0.76$) for the $D+C_6H_5S\cdot(B_2)$ channel may indicate that the S–D band dissociation proceeds on adiabatic surfaces where nuclear motions perpendicular to the S–D elongation axis are strongly coupled along the reaction coordinate. In this case a smaller translational energy and a larger internal energy of the fragment are expected. The translational energy distribution corresponding to the $D+C_6H_5S\cdot(B_2)$ channel [the inner ring of the image in Fig. 1(b)] is indeed broader compared with that of the $D+C_6H_5S\cdot(B_1)$ channel, indicating that the internal energy is more widely distributed for $C_6H_5S\cdot(B_2)$ than for $C_6H_5S\cdot(B_1)$. A theoretical interpretation of the two values of anisotropy as well as possible minimum energy pathways are detailed in the next section.

C. Minimum energy pathways leading to the S–D(H) bond dissociation from $C_6H_5SD(H)$

The absorption spectrum of thiophenol taken in *n*-hexanes shows no discernible structure in the UV region, Fig. 5. Even though earlier low-level theoretical calculations are available,[74,75] neither the energetics nor the nature of

TABLE I. The energy disposal into the $\hat{X}(B_1)$ and $\tilde{A}(B_2)$ states of the phenylthiyl radical ($C_6H_5S\cdot$) in the photodissociation of C_6H_5SD at 243 nm. (All values are in kcal/mol.)

	E_{avl} (max)[a]	$\langle E_T\rangle$	f_T (%)	E_e $(X-A)$	Yield (%)
X state (B_1)	38.11±0.30	31.26	80.9	0	43.3
A state (B_2)	30.66±0.27	20.43	60.6	7.45±0.57	56.7

[a]$E_{avl}=E_{h\nu}-D_0(S-D)-E_e$.

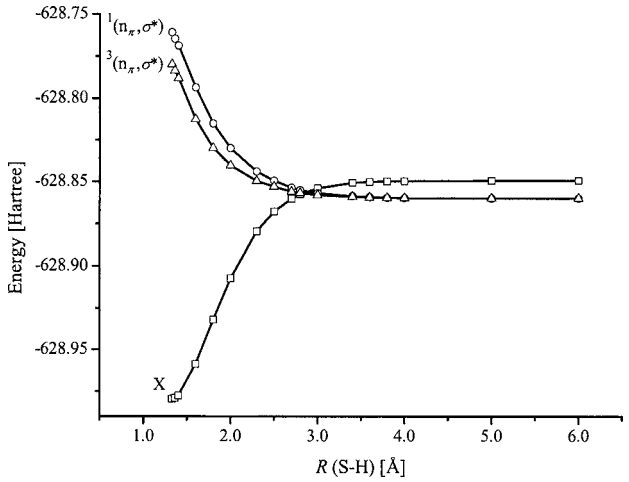

FIG. 6. Calculated potential energy curves of thiophenol as a function of S–H coordinate dissociating to the two lowest states of radical. The energy profile is obtained at the MRCI level. HOMO/SOMO is also shown.

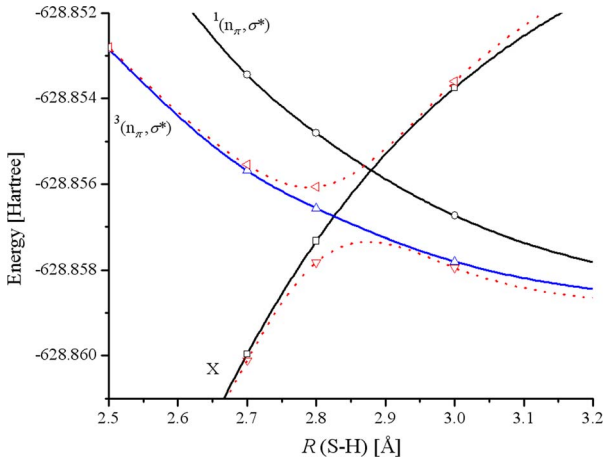

FIG. 7. (Color online) Diabatic (solid line) and spin-orbit coupled (dotted line) potential energy curves of thiophenol as a function of S–H coordinate dissociating to the two lowest states of phenylthiyl radical.

electronic transitions of thiophenol are clearly known. Therefore, attempted here is a phenomenological interpretation based on the electronic transitions leading to the ultrafast S–D bond rupture. An interesting characteristic of thiophenol is that its HOMO is a nonbonding orbital which is localized on the sulfur atom. Accordingly for the following discussion, we designate the nonbonding in-plane p orbital on sulfur, which transforms as a' by n_σ and the out-of-plane p orbital transforming as a'' by n_π. The experimental anisotropy parameter of -1 associated with the outer ring of the D ion image in Fig. 1 indicates that the corresponding $D+C_6H_5S\cdot(B_1)$ channel should be characteristic of the ultrafast S–D bond rupture. In this case, the bond rupture is initiated by a perpendicular transition of which the transition dipole moment is perpendicular to the S–D bond axis. Such a reaction proceeds along a repulsive energy profile. As for the reduced anisotropy parameter of -0.76 found for the slower D fragment associated with the inner ring in Fig. 1, there are two possible scenarios. One is that the transition dipole moment for the initial excitation may not be perpendicular to the dissociating S–D bond. One possible electronic transition is the excitation to $^1(n_\pi,\pi^*)$ state, of which the transition dipole moment lies on the molecular plane. The fact that both n_π and π^* orbital transforms as a'' means that the resulting transition dipole moment behaves like A'. In this case, depending on the angle between the transition dipole moment and the S–D bond axis, the anisotropy parameter could be reduced from the limiting value of -1. The other plausible scenario is a delayed reaction time for the $D+C_6H_5S\cdot(B_2)$ channel. The optical transition, in this case, is perpendicular to the S–D bond axis. However, the potential energy surfaces leading to $D+C_6H_5S\cdot(B_2)$ may couple with other low-lying electronic states along the reaction coordinate, resulting in a slower reaction time, hence the reduced β value. The final products are consequences of the electronic bifurcation.

In order to gain further insights into the photodissociation dynamics of the hydrogen detachment pathways, potential energy curves along the S–H dissociation coordinate are constructed from *ab initio* calculations. The details of computation were given earlier and will not be repeated here unless necessary for clarification. Figure 6 depicts the potential energy curves for thiophenol, obtained at the MRCI level, along the S–H coordinates dissociating to the two lowest electronic states of phenylthiyl radical. As can be seen, there are two repulsive states and a bound state for hydrogen detachment, corresponding to the triplet/singlet pair of (n_π,σ^*) and the ground state, $\tilde{X}$, respectively. On a diabatic curve there is a crossing between $\tilde{X}(A')$ and $^{3,1}(n_\pi,\sigma^*)(A'')$ at around $R=2.9$ Å due to symmetry conservation. Consequently, the ground state thiophenol $\tilde{X}(A')$ correlates to the excited state (B_2) of the radical whereas the excited state of $^{3,1}(n_\pi,\sigma^*)(A'')$ correlates to the ground state (B_1) of the radical at the dissociation limit. At the pump energy of 243 nm both the triplet and singlet repulsive states are accessible for photoexcitation. Due to small spin-orbit effects, however, spin-allowed transitions are expected to dominate. Then the more likely transition is to the spin allowed $^1(n_\pi,\sigma^*)$ at the initial photoexcitation. Furthermore, the anisotropy $\beta=-1$ is perfectly explained by the possibility that repulsive potential $^1(n_\pi,\sigma^*)$ is directly reached by an excitation at 243 nm. This leads to the ultrafast dissociation channel leading to the $H+C_6H_5S\cdot(B_1)$ product. Although a direct excitation to $^1(n_\pi,\sigma^*)$ seems to be the more likely candidate for the photodissociation, the energy profile for the $^3(n_\pi,\sigma^*)$ state still provides an interesting aspect of the dynamics. This becomes apparent when spin-orbit effects are taken into consideration, as shown in Fig. 7. That is, spin-orbit interaction gives rise to an avoided crossing between $^3(n_\pi,\sigma^*)$ and $\tilde{X}$. Then, both the upper $[H+C_6H_5S\cdot(B_2)]$ and lower $[H+C_6H_5S\cdot(B_1)]$ dissociation channels may well be reached if one assumes, for the former, an intersystem crossing between the singlet and triplet repulsive states before the avoided crossing. Then the longer lifetime caused by a shallow well due to a spin-orbit induced avoided crossing may be the reason for the reduced $\beta(=-0.76)$ for $H+C_6H_5S\cdot(B_2)$ product channel compared to the $H+C_6H_5S\cdot(B_1)$ channel $(\beta=-1.00)$.

Hydrogen detachment dynamics described above are mainly focused on the direct dissociation pathway accessible

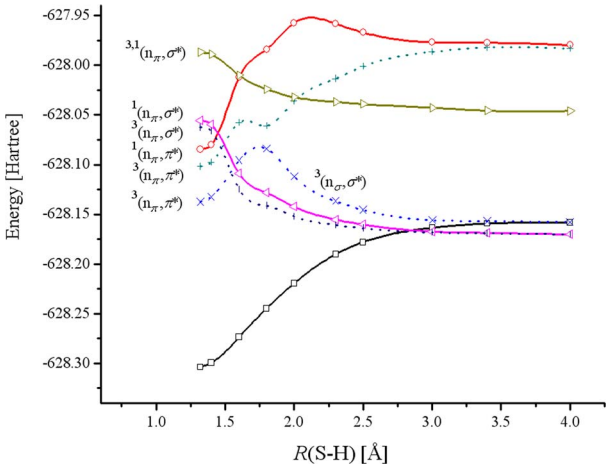

FIG. 8. (Color online) Potential energy curves of thiophenol as a function of S–H distance obtained at the MRCI level. Solid lines indicate singlet states and dotted lines the triplet states.

by excitation energy of 243 nm. The question remains, however, as to other low-lying states. For example, it is well known for phenol and phenol related clusters that the lowest excited states is $^1(\pi,\pi^*)$ which lies below $^1(\pi,\sigma^*)$ state.[45–47,76–79] We therefore elaborate on the above discussion by including other possible states. As shown in Fig. 8, $^1(n_\pi,\pi^*)$ state is found to lie below $^1(n_\pi,\sigma^*)$ and is, in fact, the lowest excited singlet state of thiophenol. More striking than the appearance of the $^1(n_\pi,\pi^*)$ below the repulsive $^{1,3}(n_\pi,\sigma^*)$ is, perhaps, the presence of the $^3(n_\sigma,\sigma^*)$ state which correlates to the $H+C_6H_5S\cdot(B_2)$ channel at dissociation limit. The nature of this pathway is more complicated than it appears on a first inspection. The repulsive part of the potential energy profile, i.e., to the right of the peak at around $R=1.7$ Å, is of the $^3(n_\sigma,\sigma^*)$ state. To the left of the peak, however, the profile becomes attractive and is characteristic of $^3(n_\pi,\sigma^*)$. As these two states do not cross each other the adiabatic potential energy profile adopts a complex shape, as depicted in Fig. 8. Although a direct excitation to $^3(n_\pi,\sigma^*)$ is unlikely as it is spin forbidden, the repulsive $^3(n_\sigma,\sigma^*)$ may still be accessed via predissociation in combination with intersystem crossing from the nearby singlet states, providing an alternative pathway to $H+C_6H_5S\cdot(B_2)$ dissociation channel. The slow D channel corresponding to the $D+C_6H_5S\cdot(B_2)$ channel thus could be the consequence of the $^3(n_\pi,\sigma^*)$ involvement in the initial electronic dephasing process. Thereafter, the wave packet undergoes either spin-orbit induced avoided crossing or follows another adiabatic surface connecting to the $^3(n_\sigma,\sigma^*)$ state to give $C_6H_5S\cdot(B_2)$ as the final product.

There is yet another possibility for reaching the two product channels. This concerns the case where the S–D bond lies out of plane of the benzene ring. Then there would be an avoided crossing between the $\tilde{X}$ and $\tilde{A}$ states dissociating along the S–D coordinates due to symmetry conservation and the two product channels are naturally reached. Although the planar configuration is the true ground state geometry according to our calculation, even a small out-of-plane bending vibration in S–D bond may prefer dissociation pathways through this mechanism.

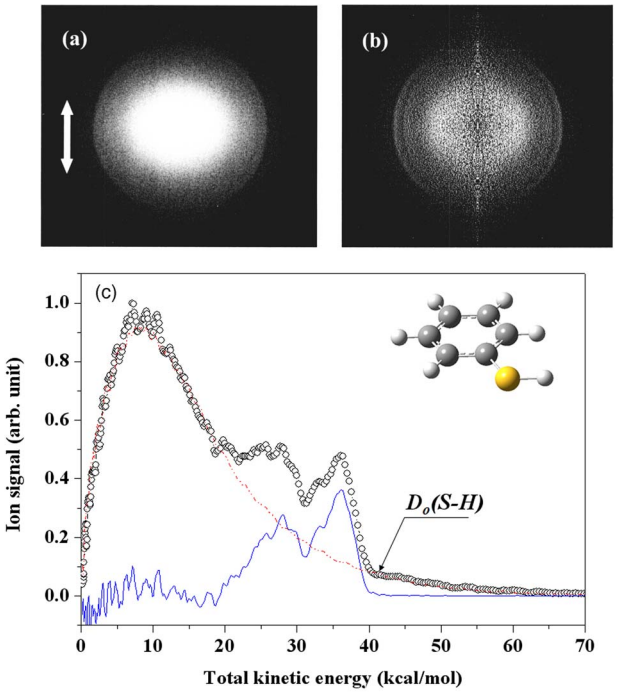

FIG. 9. (Color online) (a) 2D projection of the 3D spatial distribution of the H fragment, (b) the center slice of the reconstructed 3D distribution, and (c) the total transnational energy distribution from the C_6H_5SH photodissociation at 243 nm. The contribution only from the S–H bond dissociation is obtained by the deconvolution of the two distinct peaks out of the isotropic broad background feature. Open circles are showing the total translation energy distribution, while the (red) dotted and (blue) solid lines represent the isotropic background and anisotropic H ion signals, respectively (see the text).

D. The C–H bond dissociation from C_6H_5SH at 243 nm

The H ion image taken from the photodissociation of C_6H_5SH at 243 nm shows a broad isotropic background signal in addition to two rings, Fig. 9. Although two peaks are less distinct due to the strong broad backgroundlike feature, it is still possible to extract useful values from the experiment. By a careful deconvolution procedure assuming the smooth variation of the broad distribution, the contribution exclusively from the S–H bond dissociation of thiophenol could be nicely separated (Fig. 9). The overall shape and energy gap between two peaks are almost same as those of the D ion image in Fig. 2. The maximum value of the H translational energy of the deconvoluted distribution gives the S–H bond dissociation energy (see the following section). The broad feature is not observed in the D ion image from the C_6H_5S-D dissociation at the same wavelength. Therefore, the isotropic broad background image signal must come from the C–H dissociation of the benzene moiety. Because of the relatively poor purity of the C_6H_5SD sample ($\sim$80%), the H ion image exclusively from the C–H dissociation could not be obtained. It should be noted that the H atom scrambling between SH and CH does not occur in the excited or ground electronic state of C_6H_5SH under the experimental condition of this work.

Apart from the electronic transitions leading to the ultrafast S–H(D) bond dissociation discussed in previous sec-

TABLE II. The S–H(D) bond dissociation energy (D_0) of thiophenol in kcal/mol. (All previous reported and theoretical values are those of the S–H bond dissociation energy.)

	Method	Ref.	$D_0(S-H)$
Expt.	Velocity map ion imaging	This work	(S–D) 79.6±0.3 (S–H) 76.8±0.3
	Calorimetry[a]	35	83.3±2.0
	Estimated from pK_a, EA, and IP[b]	36	79±1
	TR-PAC[c]	37	83.51±1.08
Theor.	CASPT2 [6-31G(d,p)]	This work	82.99
	(RO)B3LYP[6-311+G(2d,2p)]+ (U)MP2(fu)[6-31G(d)]/(U)HF[6-31G(d)]	38	79.1
	ROMP2 [6-311++g(d,p)]	39	76.0
	G3(MP2)	37	82.89
	(RO)BLYP[6-311++G(2df,2p)]	40	79.49
	B3LYP [6-31G(d)]+(RO)B3LYP[6-311+G(2d,2p)]	41	77.80

[a]Estimated from a empirical correlatin technique and atomic spectroscopy at 298 K.
[b]EA electron affinity and IP ionization potential.
[c]Time-resolved photoacoustic calorimetry.

tions, the strong $^1(n_\pi,\pi^*)$ and/or $^1(\pi,\pi^*)$ transitions would also be excited at 243 nm. Similarly to the case of benzene or phenol, the C–H bond dissociation occurs in the ground electronic state (S_0) following the efficient nonradiative transitions. Since the internally hot thiophenol has enough time for its state to be completely randomized among all internal degrees of freedom prior to the bond dissociation, the energy disposal is expected to be statistical. The maximum translational energy observed in the H ion image is found to be larger than the theoretical total available energy when only one photon of 243 nm is absorbed. Therefore, the two-photon absorption of thiophenol should be heavily responsible for the isotropic broad distribution in Fig. 9. The C–H bond dissociation from C_6H_5SH is another very interesting subject to be investigated, especially since it may give a clue for disentangling complex dynamics which occur on many upper electronic states.

E. The S–H bond dissociation energy

The S–H bond dissociation energy of thiophenol has been subjected to intensive studies since thermochemical cycle of such a compound is very important in chemistry of sulfur containing compounds. Although the S–H bond dissociation energy of thiophenol has been estimated both experimentally and theoretically by many research groups,[80–86] an accurate value measured in the gas phase has not been available to date. Here we report the S–D bond dissociation energy of thiophenol-d_1 for the first time with high accuracy, giving $D_0(\mathrm{S-D})=79.6\pm0.3$ kcal/mol. This value is determined from the maximum value of the total translational energy distribution in Fig. 2. The S–H bond dissociation energy is, due to the zero-point energy difference, smaller than the S–D bond energy. Two distinct peaks above the broad background feature obviously correspond to H fragments originated from the S–H dissociation. The S–H bond dissociation energy is thus estimated from the deconvoluted H atom translational energy distribution, giving $D_0(\mathrm{S-H})=76.8\pm0.3$ kcal/mol, Fig. 9. The reported value of this work is somewhat smaller compared to all of previously reported ones, Table II. Theoretical prediction varied according to the method and basis set used for the calculation. Our CASPT2 calculation gives 82.99 kcal/mol, which is ~5% larger than the experiment, though a recent DFT calculation by Chandra *et al.*[85] gives the closer value of 79.49 kcal/mol. Selected experimental and theoretical values for the S–H bond dissociation energy of thiophenol by various methods are compiled in Table II.

V. CONCLUSION

In this paper, we presented a full account for our earlier Communication regarding photoinduced hydrogen detachment reaction of thiophenol in order to manifest a conceptual basis for a novel case of orbital alignment occurring as photoinduced products of planar aromatic systems.[62] The phenylthiyl radical species displaying a specific orbital alignment adopted at the photodissociation may serve as an example of internally aligned orbital alignment. The perpendicular alignment is found for the ground state $C_6H_5S\cdot(B_1)$ radical whereas the parallel alignment gives the electronically excited $C_6H_5S\cdot(B_2)$ state, with an energy separation of 2600 ± 200 cm^{-1}. The ultrafast photodissociation leading to the ground state $H+C_6H_5S\cdot(B_1)$ channel is most likely to proceed on a repulsive $^1(n_\pi,\sigma^*)$ profile. This may be accessed directly by a photoexcitation at 243 nm. Accordingly, the large fraction (80.9%) of the available energy goes into the translational energy of products. On the other hand, for the $H+C_6H_5S\cdot(B_2)$ channel, the triplet states play a crucial role in which the likely candidates for the minimum energy pathways are (a) the repulsive $^3(n_\pi,\sigma^*)$ state exhibiting a spin-orbit induced avoided crossing with the bound $\tilde{X}$ state and (b) the adiabatic profile characterized by $^3(n_\pi,\pi^*)\rightarrow{}^3(n_\sigma,\sigma^*)$ which provides an alternate repulsive pathway for the dissociation product of $H+C_6H_5S\cdot(B_2)$. In this case, the anisotropy value is reduced to the experimental value of -0.76 ± 0.04. The portion of translational energy in the $H+C_6H_5S\cdot(B_2)$ channel is relatively small (60.6%), which indicates that the nuclear motions perpendicular to the S–D

elongation coordinate are rather strongly coupled along the weakly bound adiabatic potential energy surfaces. The S–H(D) bond dissociation energy of thiophenol in the gas phase is accurately determined for the first time, giving $D_0(\mathrm{S-H})=76.8\pm0.3$ and $D_0(\mathrm{S-D})=79.5\pm0.3$ kcal/mol. These values are smaller than previously measured ones, and associated thermochemical values should be refined accordingly.

The intramolecular orbital alignment could introduce a new stereodynamic feature in chemical reactions. The very small energy difference between two different orbital alignments suggests that the lifetime of the upper lying $C_6H_5S\cdot$ radical should be long enough for the use in further chemical reactions. Therefore, it will be an important question whether or not the intramolecular orbital alignment of the $C_6H_5S\cdot$ radical is going to affect the chemical reactivity, for instance, in the bimolecular reaction. Since the orbital alignment is with respect to the molecular frame, the experiment for investigating stereospecific dynamics could be relatively simple since no laboratory-frame alignment or orientation will be necessary. It will be interesting to investigate the effect of orbital alignment when the phenylthiyl radical ($C_6H_5S\cdot$) forms complexes with metals. Thermodynamic differences would also be worthwhile to be investigated when two differently orbital-aligned phenylthiyl radicals approach to the two-dimensional surface for the chemical adsorption. One may be able to control the orientation of the molecule absorbed on the surface by prealigning the reactive orbital with respect to the molecular plane. The experimental demonstration of the stereospecific chemical reaction in terms of the intramolecular orbital alignment could be quite challenging. As a first step, the control of the molecule-frame orbital alignment will be pursued in the near future, for example, by tuning the excitation wavelength.

ACKNOWLEDGMENTS

The authors appreciate the great help of Dr. Kyoung-Seok Lee and Doo-Sik Ahn in the first stage of the experimental work. This work was financially supported by Korea Research Foundation (KRF-2005-070-C00063). One of the authors (Y.S.L.) acknowledges the support from a grant (06K1401-01010) from the Center for Nanoscale Mechatronics & Manufacturing, one of the 21st Century Frontier Research Programs, which is supported by the Ministry of Science and Technology, Korea.

[1] R. D. Present, Proc. Natl. Acad. Sci. U.S.A. **41**, 415 (1955).
[2] M. T. Marron, J. Chem. Phys. **52**, 4060 (1970).
[3] P. R. Brooks and E. M. Jones, J. Chem. Phys. **45**, 3449 (1966).
[4] R. J. Beuhler, Jr. and R. B. Bernstein, J. Chem. Phys. **51**, 5365 (1969).
[5] D. H. Parker, K. K. Chakravorty, and R. B. Bernstein, J. Phys. Chem. **85**, 466 (1981).
[6] H. J. Loesch and A. Remcheid, J. Chem. Phys. **93**, 4779 (1990).
[7] J. J. van Leuken, J. Bulthuis, S. Stoke, and H. J. Loesch, J. Phys. Chem. **99**, 13582 (1995).
[8] K. H. Kramer and R. B. Bernstein, J. Chem. Phys. **42**, 767 (1965).
[9] A. Lübbert, G. Rotzoll, and F. Günther, J. Chem. Phys. **69**, 5174 (1978).
[10] U. Hefter, G. Ziegler, A. Mattheus, A. Fischer, and K. Bergmann, J. Chem. Phys. **85**, 286 (1986).
[11] M. J. J. Vrakking and S. Stolte, Chem. Phys. Lett. **271**, 209 (1997).
[12] M. H. M. Janssen, J. W. G. Mastenbroek, and S. Stolte, J. Phys. Chem. A **101**, 7605 (1997).
[13] L. Cai, J. Marango, and B. Friedrich, Phys. Rev. Lett. **86**, 775 (2001).
[14] H. Stapelfeldt and T. Seideman, Rev. Mod. Phys. **75**, 543 (2003).
[15] T. P. Rakitzis, A. J. van den Brom, and M. H. M. Janssen, Science **303**, 1852 (2004).
[16] M. O. Hale, I. V. Hertel, and S. R. Leone, Phys. Rev. Lett. **53**, 2296 (1984).
[17] A. Z. Devdariani and A. L. Zagrebin, Chem. Phys. Lett. **131**, 197 (1986).
[18] A. Bahring, I. V. Hertel, E. Meyer, and H. Schmidt, Z. Phys. A **312**, 293 (1983).
[19] A. Bahring, I. V. Hertel, E. Meyer, and H. Schmidt, Phys. Rev. Lett. **53**, 1433 (1984).
[20] A. Bahring, I. V. Hertel, E. Meyer, W. Meyer, W. Spiess, and H. Schmidt, J. Phys. B **17**, 2859 (1984).
[21] J. Alford, N. Anderson, K. Burnett, and J. Cooper, Phys. Rev. A **30**, 2366 (1984).
[22] W. H. Breckenridge, C. Jouvet, and B. Soep, J. Chem. Phys. **84**, 1443 (1986).
[23] F. Alberti and A. E. Douglas, Chem. Phys. **34**, 399 (1978).
[24] A. M. Quinton and J. P. Simons, Chem. Phys. Lett. **81**, 214 (1981).
[25] P. Andresen, G. S. Ondrey, B. Titze, and E. W. Rothe, J. Chem. Phys. **80**, 2548 (1984).
[26] R. Vasudev, R. N. Dixon, and R. N. Zare, J. Chem. Phys. **80**, 4863 (1984).
[27] K.-H. Gericke, S. Klee, F. J. Comes, and R. N. Dixon, J. Chem. Phys. **85**, 4463 (1986).
[28] J. A. Guest, M. A. O'Halloran, and R. N. Zare, Chem. Phys. Lett. **103**, 261 (1984).
[29] H. Hou, S. J. Gulding, C. T. Rettner, A. M. Wodke, and D. J. Auerbach, Science **277**, 80 (1997).
[30] J. P. J. Driessen and S. R. Leone, J. Phys. Chem. **96**, 6136 (1992).
[31] A. G. Smolin, O. S. Vasyutinskii, E. R. Wouters, and A. G. Suits, J. Chem. Phys. **121**, 6759 (2004).
[32] E. R. Wouters, M. Beckert, L. J. Russell, K. N. Rosser, A. J. Orr-Ewing, M. N. R. Ashfold, and O. S. Vasyutinskii, J. Chem. Phys. **117**, 2087 (2002).
[33] D. H. Parker, H. Jalink, and S. Stolte, J. Phys. Chem. **91**, 5427 (1987).
[34] R. B. Bernstein, D. R. Herschbach, and R. D. Levine, J. Phys. Chem. **91**, 5365 (1987).
[35] J. P. Simons, J. Phys. Chem. **91**, 5378 (1987).
[36] D. H. Parker, H. Jalink, and S. Stolte, J. Phys. Chem. **91**, 5427 (1987).
[37] R. D. Levine, J. Phys. Chem. **94**, 8872 (1990).
[38] A. J. Orr-Ewing and R. N. Zare, Annu. Rev. Phys. Chem. **45**, 315 (1994).
[39] H. J. Loesch, Annu. Rev. Phys. Chem. **46**, 555 (1995).
[40] A. J. Alexander, B. Mark, K. S. Kalogerakis, and J. P. Simons, Chem. Soc. Rev. **27**, 405 (1998).
[41] A. J. Orr-Ewing, J. Chem. Soc., Faraday Trans. **92**, 881 (1996).
[42] W. G. Fateley, G. L. Carlson, and F. F. Bentley, J. Phys. Chem. **79**, 199 (1975); N. Kishimito, M. Furuhashi, and K. Ohno, J. Electron Spectrosc. Relat. Phenom. **113**, 35 (2000).
[43] E. M. Evleth, P. M. Horowitz, and T. S. Lee, J. Am. Chem. Soc. **95**, 7948 (1973).
[44] A. L. Sobolewski and W. Domcke, J. Phys. Chem. A **105**, 9275 (2001).
[45] A. L. Sobolewski, W. Domcke, C. Dedonder-Lardeux, and C. Jouvet, Phys. Chem. Chem. Phys. **4**, 1093 (2002).
[46] W. Domcke and A. L. Sobolewski, Science **302**, 1693 (2003).
[47] L. Zhenggang, W. Domcke, V. Vallet, A. L. Sobolewski, and S. Mahapatra, J. Chem. Phys. **122**, 224315 (2005).
[48] M. G. D. Nix, A. L. Devine, B. Cronin, and M. N. R. Ashfold, Phys. Chem. Chem. Phys. **8**, 2610 (2006).
[49] W. G. Hawkins and P. L. Houston, J. Chem. Phys. **73**, 297 (1980).
[50] W. G. Hawkins and P. L. Houston, J. Chem. Phys. **76**, 729 (1981).
[51] B. R. Weiner, H. B. Levene, J. J. Valentini, and A. P. Baronavski, J. Chem. Phys. **90**, 1403 (1988).
[52] M. D. Person, Q. K. Lao, B. J. Eckholm, and L. J. Butler, J. Chem. Phys. **91**, 812 (1989).
[53] X. Xie, L. Schnieder, H. Wallmeier, R. Boettner, K. H. Welge, and M. N. R. Ashfold, J. Chem. Phys. **92**, 1608 (1989).
[54] P. A. Cook, S. R. Langford, R. N. Dixon, and M. N. R. Ashfold, J. Chem. Phys. **114**, 1617 (2001).
[55] G. N. A. van Veen, K. A. Mohamed, T. Baller, and A. E. de Vries, Chem. Phys. **74**, 261 (1983).
[56] D. C. Kim, J. W. Hahn, E. S. Lee, and K. H. Jung, Chem. Phys. Lett. **265**, 573 (1997).
[57] R. E. Continetti, B. A. Balko, and Y. T. Lee, Chem. Phys. Lett. **182**, 400

(1991).
[58] S. H. S. Wilson, M. N. R. Ashfold, and R. N. Dixon, J. Chem. Phys. **101**, 7538 (1994).
[59] J. Zhang, B. Jiang, X. Yang, and J. Xie, Chem. Phys. Lett. **364**, 80 (2002).
[60] L. J. Rogers, M. N. R. Ashfold, Y. Matsumi, M. Kawasaki, and B. J. Whitaker, J. Chem. Soc., Faraday Trans. **92**, 5181 (1996).
[61] S. Nourbakhsh, H. M. Yin, C. L. Liao, and C. Y. Ng, Chem. Phys. Lett. **190**, 469 (1992).
[62] J. S. Lim, I. S. Lim, K. S. Lee, D. S. Ahn, Y. S. Lee, and S. K. Kim, Angew. Chem., Int. Ed. **45**, 6290 (2006).
[63] K. S. Lee, J. S. Lim, D. S. Ahn, K. W. Choi, and S. K. Kim, J. Chem. Phys. **124**, 124307 (2006).
[64] V. Dribinski, A. Ossadtchi, V. A. Mandelshtam, and H. Reisler, Rev. Sci. Instrum. **73**, 2634 (2002).
[65] D. H. Parker and T. J. B. Eppink, J. Chem. Phys. **107**, 2357 (1997).
[66] M. J. Frisch, G. W. Trucks, H. B. Schlegel *et al.*, GAUSSIAN 03, Revision B.03, Gaussian, Inc., Pittsburgh, PA, 2003.
[67] H.-J. Werner, P. J. Knowles, R. D. Amos *et al.*, MOLPRO, a package of *ab initio* programs, version 2002.1.
[68] K. Shibuya, M. Nemoto, A. Yanagibori, M. Fukushima, and K. Obi, Chem. Phys. **121**, 237 (1988).
[69] G. N. R. Tripathi, Q. Sun, D. A. Armstrong, D. M. Chipman, and R. H. Schuler, J. Phys. Chem. **96**, 5344 (1992).
[70] P. G. Russell, J. Phys. Chem. **79**, 1353 (1975).
[71] M. BonifaEit, J. Weiss, S. A. Chaudhri, and K.-D. Asmus, J. Phys. Chem. **89**, 3910 (1985).
[72] V. F. Plyusnin, Y. V. Ivanov, V. P. Grivin, D. Y. Vorobjev, S. V. Larionov, A. M. Maksimov, V. E. Platonov, N. V. Tkachenko, and H. Lemmetyinen, Chem. Phys. Lett. **325**, 153 (2000).
[73] D. C. Frost, F. G. Herring, A. Katrib, C. A. McDowell, and R. A. N. McLean, J. Phys. Chem. **76**, 1030 (1972).
[74] J. A. Singerman and H. H. Jaffe, J. Am. Chem. Soc. **103**, 1358 (1981).
[75] A. Scheweig, F. Diehl, K. Kesper, and H. Meyer, J. Mol. Struct. **198**, 307 (1989).
[76] C.-M. Tseng, Y. T. Lee, and C.-K. Ni, J. Chem. Phys. **121**, 2459 (2004).
[77] R. Hermann, G. R. Mahalaxmi, T. Jochum, S. Naumov, and O. Brede, J. Phys. Chem. A **106**, 2379 (2001).
[78] S. Ishiuchi, K. Daigoku, M. Saeki, M. Sakai, K. Hashimoto, and M. Fujii, J. Chem. Phys. **117**, 7077 (2002).
[79] K. Daaigoku, S. Ishiuchi, M. Sakai, M. Fujii, and K. Hashimoto, J. Chem. Phys. **119**, 5149 (2003).
[80] D. F. McMillen and D. M. Golden, Annu. Rev. Phys. Chem. **33**, 493 (1982).
[81] F. G. Bordwell, J.-P. Cheng, G.-Z. Ji, A. V. Satish, and X. Zhang, J. Am. Chem. Soc. **113**, 9790 (1991).
[82] R. M. Borges dos Santos, V. S. F. Muralha, C. F. Correia, R. C. Guedes, B. J. Costa Cabral, and J. A. M. Simões, J. Phys. Chem. A **106**, 9883 (2002).
[83] G. A. Dilabio, D. A. Pratt, A. D. LoFaro, and J. S. Wright, J. Phys. Chem. A **103**, 1653 (1999).
[84] Y. Fu, B.-L. Lin, K.-S. Song, L. Liu, and Q.-X. Guo, J. Chem. Soc., Perkin Trans. 2 **2002**, 1223.
[85] A. K. Chandra, P.-C. Nam, and M. T. Nguyen, J. Phys. Chem. A **107**, 9138 (2003).
[86] J. S. Wright, C. N. Rowley, and L. L. Chepelev, Mol. Phys. **103**, 815 (2005).